Structural, electronic and magnetic properties of the surfaces of tetragonal and cubic HfO_2

2008 New J. Phys. 10 063031

(http://iopscience.iop.org/1367-2630/10/6/063031)

New Journal of Physics
The open-access journal for physics

Structural, electronic and magnetic properties of the surfaces of tetragonal and cubic HfO_2

J I Beltrán[1], M C Muñoz[1] and J Hafner[2,3]

[1] Instituto de Ciencia de Materiales de Madrid, Consejo Superior de Investigaciones Cientificas, Cantoblanco, E-28049 Madrid, Spain

[2] Fakultät für Physik and Center for Computational Materials Science, Universität Wien, Sensengasse 8, A-1090 Wien, Austria

E-mail: Juergen.Hafner@univie.ac.at

New Journal of Physics **10** (2008) 063031 (21pp)
Received 28 April 2008
Published 25 June 2008
Online at http://www.njp.org/
doi:10.1088/1367-2630/10/6/063031

Abstract. We present *ab initio* density-functional theory (DFT) calculations of the structure and stability of the monoclinic (m), tetragonal (t) and cubic (c) phases of HfO_2 and of the stability and the structural, electronic, and magnetic properties of the polar (001) surface of t-HfO_2 and the (100) and (111) surfaces of c-HfO_2. We show that on all three surfaces, a termination by Hf leads to a metallic and non-magnetic surface, while surfaces covered by a full monolayer of O are predicted to be half-metallic and ferromagnetic, the magnetisms being induced by the Coulomb repulsion between p-holes in the O-2p valence band. In contrast, the partially reduced surfaces terminated by half a monolayer of oxygen are found to be insulating and non-magnetic. *Ab initio* statistical mechanics in combination with the DFT total-energy calculations show that the partially reduced surfaces are stable over the entire range of admissible values of the chemical potential of oxygen. Investigations of the formation of Hf vacancies on the Hf- and O-terminated surfaces of tetragonal HfO_2 demonstrate that under oxidizing conditions, the formation of Hf subsurface vacancies is energetically favored on the partially reduced O-terminated surface. The formation of Hf vacancies causes the creation of holes in the O-2p valence band and of magnetic moments on the surrounding O atoms. That the formation of near-surface Hf vacancies on the O-terminated surface is energetically favored is in contrast to a high formation energy for neutral Hf vacancies in bulk HfO_2 and suggests a cooperative mechanism between surface- and vacancy-formation. We discuss our findings in relation to recent reports on ferromagnetism in ultrathin HfO_2 films and other models for the formation of p-wave ferromagnetism.

[3] Author to whom any correspondence should be addressed.

Contents

1. Introduction

Oxides with a large bandgap are of great current interest because of many potential applications. A particularly important class of oxides are those with a high dielectric constant, or 'high-K' oxides [1]–[3]. These oxides will replace SiO_2 as the gate dielectric in complementary metal oxide semiconductor (CMOS) devices. The need to replace SiO_2 arises from the fact that due to the reduced dimensions of the devices the thickness of the gate oxide layer becomes so thin that conduction electrons can tunnel directly through the insulating layer. This can be avoided by replacing SiO_2 as a gate material by an oxide with a higher dielectric constant. Candidates are HfO_2, ZrO_2 or La_2O_3. Other classes of large-gap oxides of current technological interest are transparent conducting oxides for use in flat panel displays and low-emissivity windows [4]. They should have a bandgap larger than 3 eV and be susceptible to doping to become highly conducting—potentially useful materials are ZnO, In_2O_3 and SnO_2. The last material and TiO_2 are also of interest as gas sensors and catalysts [5, 6].

A very intriguing recent discovery was that semiconducting or insulating oxides, such as ZnO, TiO_2 or SnO_2 can become ferromagnetic at room temperature if doped with a few per cent of transition-metal cations [7]–[13]. These observations are incompatible with a picture based on magnetic moments carried by the d-electrons of the transition-metal cations and coupled via nearest-neighbor super-exchange interactions, because the doping level is definitely below the percolation threshold and in many cases the moment per cation exceeds the limiting value for the spin-moment set by Hund's rule. The origin of ferromagnetic ordering has been assigned to indirect d-electron exchange interaction mediated by defects [14].

Even more challenging, however, is the observation that room-temperature ferromagnetism can exist also in undoped insulating thin oxide films and nano-particles (TiO_2, HfO_2 and In_2O_3) [13], [15]–[18]. It has been proposed that the origin of magnetism is associated with the existence of a small concentration of intrinsic point defects—isolated cation vacancies lead to the formation of high-spin defect sites [18, 19]. This argument relates to the established fact that two-electron defect centers in oxides (such as a neutral cation vacancy—a V^0 center) can have a spin-triplet ground state or low-lying excited state [20, 21]. Alternatively, it has

been proposed [22] that hole-doping, i.e. the substitution of Hf by an element with a lower valence (K, Sr and Al) can lead to the formation of a small magnetic moment on the oxygen sites. For the magnetic ordering in systems, where the magnetic moment is carried by atoms without d- or f-electrons, Coey [11] has coined the term 'd^0 ferromagnetism'—other materials belonging to this class are irradiated graphite [23] and non-stoichiometric CaB_6 [24]. Since the undoped bulk oxides are diamagnetic and there are no impurities, it was suggested that the thin-film form of the oxides is instrumental to the observed ferromagnetic ordering [18]. Furthermore, it was reported that the magnetization does not scale with film thickness, but depends on the surface area. A magnetic moment of 100–400$\mu_B\,nm^{-2}$ was reported [11]. In a recent paper [25], we have reported that on the oxygen-terminated polar surfaces of ZrO_2, Al_2O_3 and MgO, large spin-moments are formed on the terminal oxygen atoms such that on top of the non-magnetic insulating bulk a half-metallic magnetic surface develops. Although the fact that the same phenomenon is predicted to occur on the surfaces of three different oxides suggests that the mechanism has general validity, it is a bit unfortunate that the theory refers to oxides for which thin-film magnetism has not been reported as yet. For this reason, we return to the task and present here a detailed density-functional investigation of the stability, structure, and of the electronic and magnetic properties of the polar low-index surfaces [(100) and (111)] of cubic HfO_2 and of the (001) surface of tetragonal HfO_2. Very recently, Mukhopadhyay *et al* [26] have reported *ab initio* calculations of the structural and electronic properties of the surfaces of monoclinic hafnia. However, these calculations did not include a possible surface-induced formation of magnetic moments. The investigations of the surfaces of the tetragonal and cubic polymorphs is interesting because recent investigations of the structure of atomic layer deposited films demonstrated a preferential formation of the tetragonal phase [27] or at least a coexistence of the tetragonal and monoclinic phases [28] in ZrO_2 and HfO_2 films.

Our paper is organized as follows: in section 2, we briefly introduce the density-functional methodology used in our study; in section 3, we summarize the results for the three isomorphs of bulk HfO_2 stable at ambient pressure, including a detailed comparison with earlier theoretical studies and with experiment. Section 4 presents our results for the stability, structure and for the electronic and magnetic properties of the polar (001) surface of tetragonal HfO_2 and of the polar low-index [(100) and (111)] surfaces of cubic HfO_2. The influence of point defects on the surface properties of tetragonal HfO_2 is discussed in section 5. In section 6, we summarize our results and we discuss our results in relation to other models proposed to explain the existence of 'd^0 ferromagnetism'.

2. Methodology

The calculations have been performed using the Vienna *ab initio* simulation package (VASP) [29]–[31][4], which performs a variational solution of the Kohn–Sham equations in a plane-wave basis set. The electron–ion interaction is described using the projector-augmented wave (PAW) method introduced by Blöchl [32] as modified by Kresse and Joubert [33]. Electronic exchange and correlation are described in the generalized gradient approximation, using the functional proposed by Perdew–Burke–Ernzerhof (PBE) [34]. The plane-wave basis set contained components with a kinetic energy of up to $E_{cut} = 354\,eV$—with this cut-off, a good convergence of the structural energy differences between the cubic, tetragonal and

[4] Detailed information on VASP may be found on the website: http://cms.mpi.univie.ac.at/vasp.

monoclinic phases of HfO_2 could be achieved (see also the following section). For the Brillouin zone (BZ) integrations a $12 \times 12 \times 12$ Monkhorst–Pack grid [35] over the BZ of the primitive cell has been used for bulk cubic HfO_2. For the tetragonal and monoclinic phases, we used a cell containing four formula units, BZ integrations were performed over a $6 \times 6 \times 6$ mesh. Geometric relaxations were performed with a quasi-Newton algorithm using the exact Hellmann–Feynman forces, with a criterion for stopping the structural optimization if residual forces are smaller than 0.05 eV $Å^{-1}$.

The (001) surface of tetragonal HfO_2 and the (100) and (111) surfaces of the cubic phase have been modeled by periodically repeated slabs containing up to 11 HfO_2 layers separated by a vacuum layer of at least 15 Å. We use a (1×1) surface cell containing just one formula unit per cell. For the spin-polarized calculations of the magnetically ordered surface, the spin interpolation formula of Vosko, Wilk and Nusair was used [36]. The BZ integrations have been performed on $4 \times 4 \times 1$ k-point meshes, convergence has been verified by test-calculations using $8 \times 8 \times 1$ grids. Both non-stoichiometric symmetric Hf- and O-terminated slabs and polar asymmetric stoichiometric slabs (in this case including dipolar energy corrections) have been used. To reduce the computational workload, the plane-wave cut-off has been reduced to 283 eV for the surface calculations. We have verified that the reduction of the cut-off energy does not affect the accuracy of our results in any significant way.

3. Phase stability of HfO_2

HfO_2 is a ceramic compound which exists at ambient pressure in three different crystallographic phases: monoclinic (space group $P2_1/c$) HfO_2 is the stable low-temperature phase, transforming martensitically to a tetragonal phase (space group $P4_2nmc$) at about 2000 K and further to a cubic fluorite-type (space group $Fm3m$) lattice at 2870 K. In addition, two orthorhombic high-pressure phases (space groups $Pbca$ and $Pnma$) have been identified [37, 38]. The low-pressure forms of HfO_2 have a wide range of potential applications, ranging from solid fuel cell electrolytes and microelectronics gate dielectrics to catalyst supports. In addition, it has been suggested that the high-pressure polymorphs quenched to ambient conditions might be useful superhard materials. The high-temperature phases (tetragonal and cubic) may be stabilized by doping or in thin films by epitaxial constraints imposed by the substrate.

During recent years, a number of *ab initio* density-functional investigations of the phase-stability of HfO_2 have been performed [39]–[42], together with the experimental information this forms a database for assessing the accuracy of our calculations. Our calculated structural parameters, bulk moduli and structural energy differences for the monoclinic, tetragonal and cubic phases of HfO_2 are compiled in table 1, together with the available experimental information and the results of the four most recent theoretical studies. Like the present work, these investigations are also based on density-functional theory (DFT). Jaffe *et al* [39] used an older version of VASP based on ultrasoft pseudopotentials (US-PP) instead of the all-electron PAW method, and the Perdew–Wang (PW) [50] instead of the PBE functional. Kang *et al* [40] used a norm-conserving pseudopotential (NC-PP) and the PBE functional. Zhao and Vanderbilt [41] also used NC-PPs and the PBE functional. The calculations of Foster *et al* [42] have been performed using the US-PP version of the VASP and the PBE functional. Hence, a comparison of these results allows to assess the influence of the choice of the gradient-corrected exchange-correlation functional and of the pseudopotential. One should remember that for compounds involving transition-metal atoms, basis-set convergence is more easily achieved

Table 1. Structural parameters (in Å), volume per formula unit (in Å^3, bulk moduli B (in GPa), structural energy differences ΔE (in eV formula unit^{-1}), and bandgaps E_g (in eV) for the cubic, tetragonal and monoclinic phases of HfO_2—present results are compared with earlier calculations and with experiment.

	Present work	[39] US-PP, PW	[40] NC-PP, PBE	[41] NC-PP, PBE	[42] US-PP, PBE	Exp.[a]	Exp.[b]
Monoclinic volume	35.13	34.81	36.39	38.01	34.81	34.62	34.67
a	5.148	5.128	5.215	5.291	5.132	5.117	–
b	5.191	5.191	5.293	5.405	5.189	5.175	–
c	5.334	5.297	5.350	5.366	5.307	5.291	
β	99.69	99.71	99.73	97.92	99.78	99.22	
B	238	152	–	–	–	–	282, 145
ΔE	0.0	0.0	–	–	–	–	
E_g	4.10	3.80	3.6	–	4.1	5.7	
Tetragonal volume	33.72	33.30	34.82	37.74	33.12	35.07	
a	3.591	3.578	3.655	3.747	3.578	3.642	
c	5.228	5.200	5.220	5.373	5.181	5.289	
c/a	1.455	1.453	1.428	1.434	1.448	1.452	
δ	0.055	0.055	0.033	0.041	0.051	–	
B	244	201	183	–	–	–	
ΔE	0.163	0.156	0.135	–	0.160	–	
E_g	4.85	4.45	–	–	–	–	
Cubic volume	32.71	32.45	34.10	36.15	32.49	32.77	
a	5.076	5.063	5.148	5.248	5.070	5.080	
B	258	260	257	–	–		
ΔE	0.260	0.237	0.169	–	0.240		
E_g	3.95	3.70	–	–	–	5.6–6.0	

[a] See [43] for monoclinic, [44] for tetragonal (high-temperature results at $T = 1800\,^{\circ}C$), [45] for cubic HfO_2. Bandgap of monoclinic phase after [46], of the cubic phase after [47].
[b] See [48, 49] for monoclinic HfO_2.

using ultrasoft than with NC-PPs. In contrast, the present work is based on the all-electron PAW method. In general, well-converged US-PP and PAW calculations yield results in excellent agreement, but for systems with an appreciable overlap between core and valence electron densities the PAW method allows to achieve a higher accuracy because, as the exchange-correlation energy is calculated for the correct all-electron density, no elaborate nonlinear core-corrections [51] to the valence–core interactions are required. It has been demonstrated that this may be relevant in particular for magnetic systems [33].

For the cubic phase, we note good agreement of the three calculations based on either the PAW approach or US-PP's (present work and [39, 42]) with experiment [45], while the calculations using NC-PP's consistently overestimate the volume. The difference between the results achieved with PBE and PW functionals is small. The present calculations with the PAW method yield a slightly larger equilibrium volume (by about 1%) than the previous calculations based on US-PP. A similar conclusion applies to the theoretical calculations for the tetragonal

Table 2. Dimensionless internal coordinates of Hf and O1 and O2 atoms in the monoclinic phase.

	Present work	[39] US-PP, PW	[40] NC-PP, PBE	[41] NC-PP, PBE	[42] US-PP, PBE	[43] Exp.
Monoclinic volume	35.13	34.81	36.39	38.01	34.81	34.62
x(Hf)	0.276	0.277	0.277	0.276	0.277	0.276
y(Hf)	0.042	0.043	0.042	0.039	0.044	0.040
z(Hf)	0.208	0.209	0.207	0.209	0.209	0.208
x(O1)	0.066	0.074	0.076	0.089	0.070	0.074
y(O1)	0.327	0.342	0.343	0.367	0.333	0.332
z(O1)	0.349	0.337	0.335	0.317	0.345	0.347
x(O2)	0.449	0.448	0.447	0.447	0.448	0.449
y(O2)	0.757	0.759	0.759	0.762	0.758	0.759
z(O2)	0.477	0.481	0.483	0.488	0.478	0.480

and monoclinic phases (but it has to be pointed out that for the tetragonal phase, only high temperature data are available for comparison). For the tetragonal phase, calculations using US-PP or PAW potentials achieve a higher accuracy for the axial ratio and the parameter δ determining the atomic positions within the unit cell. For the monoclinic phase, table 2 lists in addition the dimensionless internal coordinates for the three crystallographically inequivalent sites. Again, we note excellent agreement with experiment. For the present calculations, the largest difference in an individual coordinate is 0.04 Å, the average error is 0.01 Å. Slightly larger differences appear for the earlier pseudopotential calculations.

The total and partial electronic densities of states (DOSs) of all three polymorphs of HfO_2 are shown in figure 1. For the energy gap of monoclinic HfO_2, we calculate a value of 4.1 eV, in agreement with the work of Foster *et al* [42], but larger by up to 0.5 eV than reported in the earlier pseudopotential studies [39, 40]. However, the gap width is considerably underestimated compared to the experimental value of 5.7 eV, a characteristic of DFT. A wider gap of 4.85 eV is predicted for the tetragonal phase, while the cubic phase has a narrower gap of only 3.95 eV. In all three polymorphs, the DOS of the valence band is dominated by the O-2p orbitals, whereas the conduction band has almost pure Hf-5d character. Hence, HfO_2 is essentially a charge-transfer insulator.

4. Surface properties of HfO_2

In the following, we shall present the results for the surface properties of tetragonal and cubic hafnia. As described above, the surfaces are modeled by periodically repeated slabs with a (1×1) surface cell containing one formula unit per layer. To check the convergence, the thickness of the slabs has been varied between 3 and 11 HfO_2 layers.

Our study covers the (001) surface of tetragonal(t) HfO_2 and the (100) and (111) surfaces of cubic HfO_2. All these surfaces are polar and can be terminated either by a Hf- or an O-layer. As the O-surface layer contains two atoms per (1×1) cell, there exists also the possibility to choose a partially reduced surface termination with a single O atom in the surface cell. We shall use

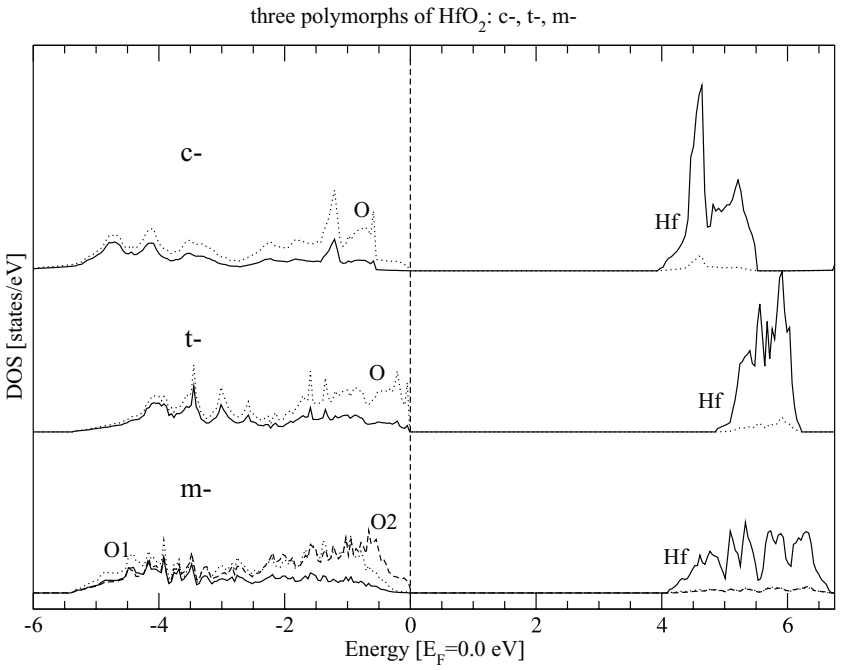

Figure 1. Partial electronic DOS of monoclinic, tetragonal and cubic HfO_2. Full lines represent the partial Hf-DOS, dotted and dashed lines the partial O-DOS (cf text).

the nomenclature t-$(001)_{OO}$, t-$(001)_{O}$ and t-$(001)_{Hf}$ (and correspondingly for the other surface orientations and the cubic phase) to designate the fully oxygen-covered or OO-terminated, the partially reduced or O-terminated and the Hf-terminated surfaces. The calculations have been performed both for symmetric slabs with the same termination at the upper and lower surfaces, and for asymmetric stoichiometric slabs with one Hf- and one O-terminated surface and applying dipolar corrections. In each calculation, the lower half of the slab has been frozen in a bulk-like geometry, whereas in the upper half, the positions of the atoms have been allowed to relax. For all surfaces, both non-magnetic and spin-polarized calculations have been performed to determine the magnetic energy difference between the paramagnetic and ferromagnetic surfaces.

The stability of the surfaces depends on the partial pressure of oxygen and hence requires the calculation of the surface free energy as a function of the chemical composition of the solid and the partial pressure in the atmosphere above the surface. For a surface in thermal equilibrium with the oxygen gas, the surface free energy is given by [52]

$$\sigma = \left[G(T, p, \{n_x\}) - \sum_x n_x \mu_x(T, p_x) \right] \Big/ A, \tag{1}$$

where G is the Gibbs free energy, n_x the number of particles of type x $[x = \mathrm{Hf}, \mathrm{O}]$ in the solid, μ_x and p_x are the chemical potential and the partial pressure of the species x and A is the total surface area. The Gibbs free energy can be approximated by the internal energy $E(T = 0, p = 0, n_x)$ from the DFT calculations. For HfO_2, thermal equilibrium between bulk

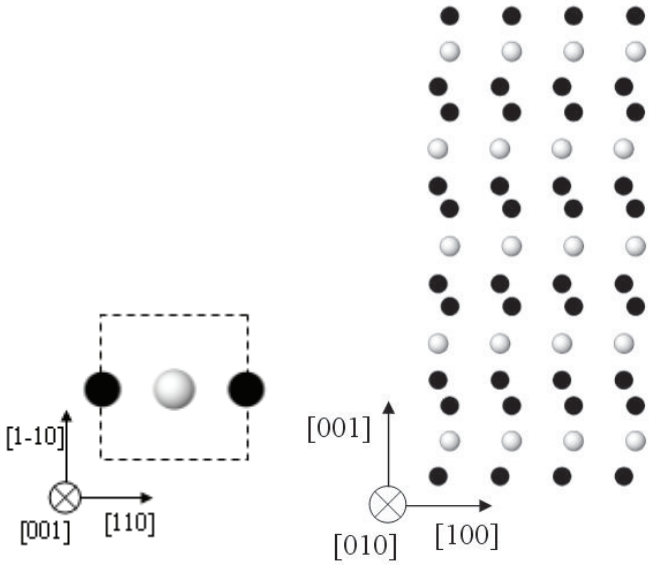

Figure 2. Top and side views of the relaxed O-terminated (001) surface of t-HfO_2. Black dots represent oxygen and gray dots hafnium atoms.

and surface requires that

$$\mu_{\mathrm{Hf}} + 2\mu_{\mathrm{O}} = E_{\mathrm{HfO_2}}. \tag{2}$$

In this approximation, the surface free energy depends on the chemical potential of oxygen only,

$$\sigma = [E\{n_x\} - n_{\mathrm{Hf}} E_{\mathrm{HfO_2}} - (n_{\mathrm{O}} - 2n_{\mathrm{Hf}})\mu_{\mathrm{O}}]/A. \tag{3}$$

The chemical potential of oxygen can vary over the range

$$\tfrac{1}{2}[E_{\mathrm{HfO_2}} - E_{\mathrm{Hf}}] \leqslant \mu_{\mathrm{O}} \leqslant \tfrac{1}{2}E_{\mathrm{O_2}}, \tag{4}$$

the lower limit is set by the reduction of HfO_2 to metallic Hf, and the upper limit by the condensation of molecular oxygen. If the chemical potential is measured relative to the binding energy of molecular oxygen, $\Delta\mu_{\mathrm{O}} = \mu_{\mathrm{O}} - \frac{1}{2}E_{\mathrm{O_2}}$, this relation reads

$$\tfrac{1}{2}\left[\Delta E^{\mathrm{f}}_{\mathrm{HfO_2}}\right] \leqslant \Delta\mu_{\mathrm{O}} \leqslant 0, \tag{5}$$

where $\Delta E^{\mathrm{f}}_{\mathrm{HfO_2}} = E_{\mathrm{HfO_2}} - E_{\mathrm{Hf}} - E_{\mathrm{O_2}}$ is the energy of formation of HfO_2.

4.1. The (001) surface of tetragonal HfO_2

4.1.1. Structure and stability of the O- and Hf-terminated (001) surfaces. The HfO_2 unit cell of the (001) surface of t-HfO_2 contains just one atom for a Hf-terminated surface, but two atoms on an O-terminated surface. A schematic view of the (001) surface is shown in figure 2. In this case, a surface retaining a bulk-like geometry is buckled, the extent of the buckling is described by the parameter δ of the tetragonal crystal structure (see table 1). The difference in the z-coordinates of the two surface oxygen atoms is $\Delta z = 2 \times \delta \times c = 0.29$ Å, corresponding to different distances between the O atoms and the Hf-atom in the next layer of 2.40 and 2.07 Å, the O–O distance is 2.60 Å. The results for the surface energies, relaxation energies and relaxed interatomic distances of the Hf-, OO- and O-terminated (001) surfaces of tetragonal HfO_2 are

Table 3. Surface energy E_{surf} (in eV Å^{-2}), relaxation energy E_{rel} (in eV cell^{-1}), oxygen–oxygen distances d(O–O) and oxygen–hafnium distances d(O–Hf) (all distances are given in Å) for the Hf-, OO- and O-terminated (001) surfaces of tetragonal HfO_2 as a function of the slab-thickness.

		Hf-term. 3 layers	Hf-term. 5 layers	Hf-term. 11 layers	OO-term. 3 layers	OO-term. 5 layers	OO-term. 11 layers	O-term. 11 layers
E_{surf}		0.609	0.608	0.604	0.202	0.213	0.209	0.078
E_{relax}		0.067	0.065	0.069	0.501	0.406	0.422	0.123
OO	d(O–O)	–	–	–	2.54	2.54	2.54	–
	d(O–Hf)	–	–	–	2.07, 2.06	2.06, 2.12	2.07, 2.12	2.02
Hf	d(Hf–O)	2.06, 2.27	2.06, 2.28	2.06, 2.28	2.23, 2.38	2.19, 2.42	2.19, 2.40	2.02, 2.46
OO	d(O–O)	2.57	2.57	2.57	2.55	2.57	2.56	2.65
	d(O–Hf)	2.32, 2.10	2.33, 2.10	2.33, 2.10	2.24, 2.10	2.27, 2.07	2.27, 2.08	2.48, 2.04
Hf	d(Hf–O)	2.09, 2.37	2.08, 2.37	2.08, 2.37	2.07, 2.40	2.10, 2.41	2.10, 2.39	2.42, 2.05
OO	d(O–O)	2.59	2.59	2.59	2.60	2.59	2.59	2.62
	d(O–Hf)	2.37, 2.08	2.37, 2.08	2.37, 2.08	–	2.37, 2.07	2.36, 2.07	2.05, 2.43
Hf	d(Hf–O)	2.07, 2.40	2.08, 2.40	2.07, 2.39	–	2.07, 2.40	2.08, 2.41	2.40, 2.06
OO	d(O–O)	2.60	2.60	2.60	–	2.60	2.60	2.60
	d(O–Hf)	2.40, 2.07	2.40, 2.07	2.39, 2.08	–	–	2.40, 2.07	2.06, 2.40
Hf	d(Hf–O)	–	2.07, 2.41	2.07, 2.40	–	–	2.06, 2.41	2.40, 2.07
OO	d(O–O)	–	2.60	2.60	–	–	2.61	2.60
	d(O–Hf)	–	–	2.40, 2.07	–	–	2.41, 2.07	2.06, 2.40

compiled in table 3, as calculated for slabs containing 3, 5 and 11 HfO_2 layers. Surface energies are quoted for the upper limiting value for the chemical potential of oxygen ($\mu_O = \frac{1}{2}E_{O_2}$). O–O distances are intra-planar distances within a slightly buckled oxygen layer, O–Hf and Hf–O distances are inter-planar distances. We note that the energies and interatomic distances converge quickly with the slab-thickness and that the relaxation affects essentially only the first three HfO_2 layers. On both surfaces, the top layer relaxes inward, as reflected by the contraction of the distances between atoms in the surface and subsurface layers. The oxygen-terminated surfaces are subject to a much stronger relaxation than the Hf-terminated surface. Due to the relaxation, the buckling of the surface O-layer on the OO-terminated surface disappears almost completely, the gain in surface energy by relaxation is almost one order of magnitude larger than for the metal-terminated surface. A similar result has also been found by Eichler and Kresse [53] for the surface of tetragonal ZrO_2. For the O-terminated surface, the single surface O-atom moves into a position directly above the underlying Hf-atom.

Figure 3 shows the surface free energy as a function of the oxygen chemical potential. The symmetric slabs representing the Hf- and OO-terminated surfaces are non-stoichiometric and hence show a strong dependence of the surface free energy on the chemical potential, while that of the stoichiometric slabs representing the partially reduced O-terminated surface remain constant. The partially reduced O-terminated surface is found to be stable over the entire admissible range of the chemical potential. The magnetic energy reduces the energy difference between the fully O-covered and the partially reduced surface (see the following subsection), but this is not sufficient to stabilize a full coverage of the surface by oxygen.

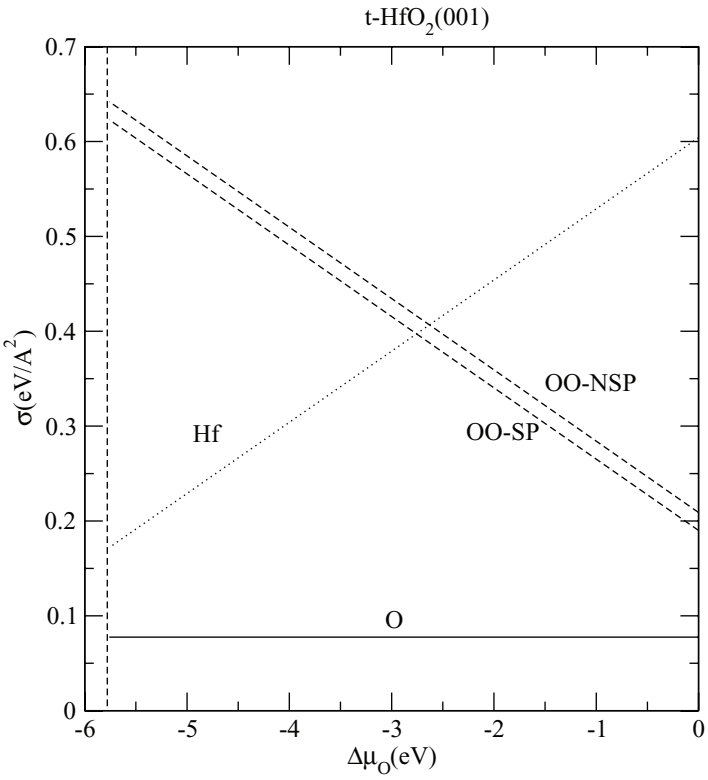

Figure 3. Surface free energies of the Hf- and OO-terminated and of a partially reduced O-terminated (001) surface of tetragonal HfO_2 as a function of the oxygen chemical potential (calculated relative to molecular oxygen). Vertical lines represent the upper and lower limits of the chemical potential. For the O-terminated surfaces, the energies of both the non-magnetic and the ferromagnetic states are displayed (cf text).

4.1.2. Magnetic and electronic structure of the oxygen-terminated (001) surface. If a spin-polarized calculation is performed, the OO-terminated surface becomes ferromagnetic, while the partially reduced O-terminated and the Hf-terminated surfaces remain non-magnetic. The spin-polarized calculations have been performed for slabs with 5 to 11 HfO_2 layers, but the thickness dependence is only very modest: the energy difference between the non-magnetic and the ferromagnetic slab increases from 0.78 to 0.79 eV cell^{-1}, the magnetic moments of the two inequivalent O atoms in the surface layer increase from 1.07 and $0.52\mu_B$ to 1.08 and $0.53\mu_B$, respectively, as the thickness of the slab is increased from 5 to 11 layers. The Hf atoms in the subsurface layer carry a modest magnetic moment of $-0.06\mu_B$ oriented antiparallel to the moments on the oxygen atoms. The magnetic polarization extends also to subsurface oxygen atoms, the moments in the second O-layer are 0.23 and $0.02\mu_B$, in the third O-layer one of the oxygen atoms carries a magnetic moment of $0.04\mu_B$, while the second atom is essentially non-magnetic. The surface relaxation has a modest influence on the magnetic properties. On a non-relaxed, bulk-terminated surface the oxygen atoms carry moments of 1.26 and $0.54\mu_B$, respectively. This shows that the inward-relaxation of the surface oxygens and the reduction of the surface-buckling act against the formation of a magnetic moment.

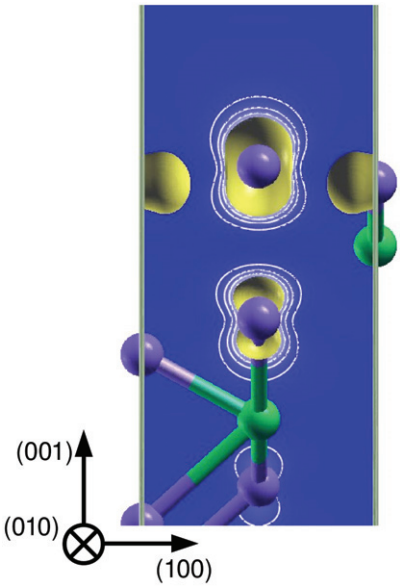

Figure 4. Contour plot of the magnetization density located at the O-atoms of the double O-terminated (001) surface of tetragonal HfO_2. The light (yellow) contours show a contour calculated at a density of 0.2 electrons $Å^{-3}$, the contour lines show the magnetization density in a plane perpendicular to the surface and to the viewer, with contour intervals of 0.05 electrons $Å^{-3}$. Dark (blue) balls represent O-atoms and light (green) balls Hf-atoms.

It is also interesting to analyze the spatial distribution of the magnetization density centered on the oxygen atoms of the double O-terminated surface—this is illustrated in figure 4 in the form of a contour plot. It is interesting to point out that the magnetization density on the site carrying the largest moment is anisotropic—the iso-density contour has the form of an ellipsoid with the long axis perpendicular to the surface.

An analysis of the layer-resolved spin-polarized electronic DOSs explains why the Hf-terminated and the partially reduced surfaces remain non-magnetic, while surface-induced ferromagnetic moments on the oxygen sites are formed on the OO-terminated surface. In the bulk, the 2p-band of oxygen is completely filled by the transfer of electrons from Hf (which is reduced to a tetravalent Hf^{4+} cation) to oxygen, for the O^{2-} anion the p-shell is completed. Hence the valence band is dominated by O-2p orbitals, while the conduction band is formed by Hf-5d states. The bandgap is a classical charge-transfer gap.

Figure 5 shows the layer resolved local DOSs for all three surface terminations. For each graph, the top panels show the local DOS for atomic sites in the surface (S) and subsurface (S-1) layer, the lowest panels (labeled S-4) show the local DOS for atoms in the first non-relaxed layer in the center of the slab—this is the closest approximation to the local DOS in the bulk for these models. On the Hf-terminated surface all four valence electrons cannot be transferred to neighboring O atoms. The excess electrons which cannot be accommodated in the fully occupied O-2p valence band occupy d-states close to the conduction band minimum—this explains why this termination is energetically rather unfavorable and stabilized only under strongly reductive conditions. This surface is metallic and non-magnetic. The gap between the highest occupied O-2p band and the lowest occupied Hf-5d state is narrowed to about 2.5 eV.

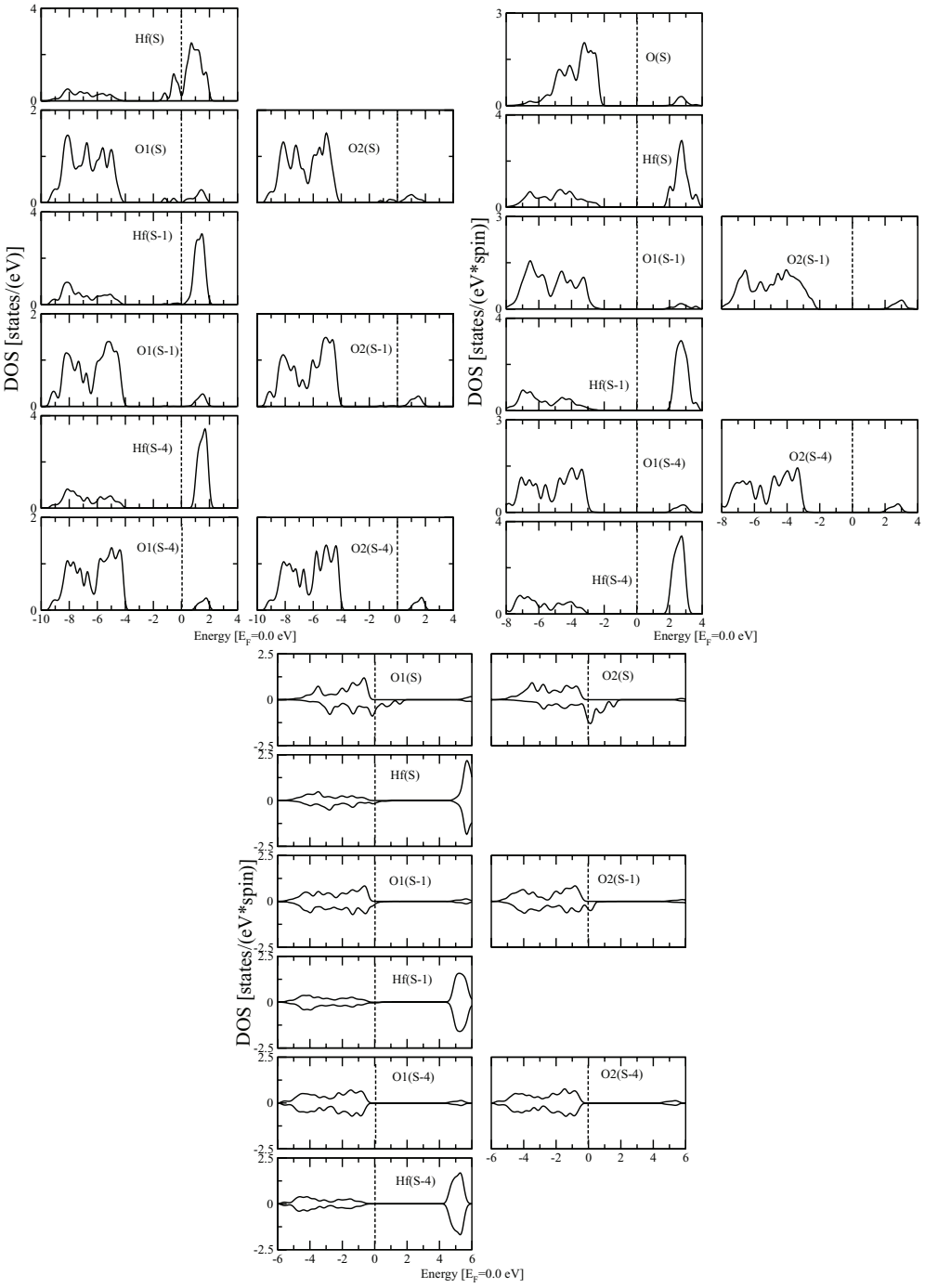

Figure 5. Layer-resolved local electronic DOS of the Hf-terminated (top, left), the single O-terminated (top, right), and the double O-terminated (bottom, center) (001) surfaces of tetragonal HfO_2. For the double O-terminated surface the spin-polarized state is shown. Note that the surface covered with a full O-monolayer is half-metallic and ferromagnetic, the surface covered by half a monolayer of oxygen is insulating and non-magnetic, whereas the Hf-terminated surface is metallic and non-magnetic. The label S identifies the surface layer, S-1 the first subsurface layer and so forth (cf text).

On the partially reduced O-terminated surface, the electrons transferred from the Hf-atoms to the remaining single O-atom per cell are sufficient to complete the filling of the O-2p band. The surface remains insulating and non-magnetic, with a gap that is only slightly reduced compared to the bulk.

On the OO-terminated surface a complete filling of the 2p-band is impossible, because the Hf-atoms in the subsurface layer donate only two electrons to the upper O-layer, two electrons being required to saturate the O-2p states in the subsurface layer. The partially occupied O-2p band is unstable against spin-splitting which is favored by (i) Hund's rule coupling favoring a parallel alignment of the spins of the p-electrons and (ii) the on-site Coulomb repulsion between two holes in an oxygen p-orbital. For the on-site Coulomb repulsion between two holes in an O-2p orbital, Efimov *et al* [21] reported a value of $U_{pp} \sim 5$–7 eV, which is slightly larger than the band width of about 5.5 eV of HfO_2 and comparable to the Coulomb repulsion between d-electrons of strongly correlated transition-metal compounds [54, 55].

The layer-resolved DOS's shown in figure 5 confirm this picture. We find that the OO-terminated surface is half-metallic and ferromagnetic: the 2p-band of the majority spins is completely filled, whereas the 2p-band of the minority spins is up-shifted by about 2 eV. The Fermi level falls into a region with a substantial minority-spin DOS. Almost no spin-splitting is detectable on the near-surface Hf atoms, and the exchange-splitting is strongly reduced already for the oxygen atoms in the second layer. The anisotropic magnetization density arises from a preferential depletion of the O-p orbitals extending perpendicular to the surface, while the in-surface p-orbitals remain spin-compensated. It is important to note that the mechanism leading to the formation of a ferromagnetic surface is based on the creation of holes in the O-2p band, as previously reported for ZrO_2 surfaces [25].

4.2. Low-index surfaces of cubic HfO_2

Of the three low-index surfaces of cubic HfO_2, the surface layer of the (110) surface has the same stoichiometry as the bulk, whereas the (111) and (100) surfaces are polar and can be terminated either by hafnium or oxygen—for the O-terminated surfaces we can consider either a full monolayer coverage of O or a partially reduced surface covered by only half a monolayer of O. On the (100) surface, both Hf and O are arranged in layers parallel to the surface, while on the (111) surface the OO-terminated surface is again strongly buckled. Sketches of both surfaces are displayed in figure 6. In the following, we shall investigate all three possible terminations for the two polar surfaces. The computational setup is essentially the same as described above for the surface of tetragonal HfO_2, only the converged results for the thickest slabs will be discussed in the following.

4.2.1. Structure and stability of Hf- and O-terminated surfaces. The surface free-energies calculated for $\Delta\mu_O = 0$, i.e. under strongly oxidizing conditions, and the energy gain by relaxation of the low-index surfaces of cubic HfO_2 are listed in table 4, the free energies as a function of the oxygen chemical potential are shown in figure 7. The resulting picture is similar to that discussed above for the tetragonal phase, but for the (111) surface the difference in the surface energies of the fully oxygen-covered and the partially reduced surface is larger than on the surface of the tetragonal phase: for both the (100) and the (111) surfaces the partially reduced single O-terminated surface is stable over the entire range of the chemical potential of oxygen. Only in the limit of very strongly oxidizing or reducing conditions the fully O-terminated or

Table 4. Surface energy $E_{\text{surf}}\Delta\mu_{\text{O}} = 0$, relaxation energy E_{rel} of the Hf-, OO- and O-terminated (100) and (111) surfaces of cubic HfO_2.

	(100) Hf-term.	(100) OO-term.	(100) O-term.	(111) Hf-term.	(111) OO-term.	(111) O.term.
E_{surf} (eV Å^{-2})	0.600	0.183	0.051	0.661	0.268	0.046
E_{relax}(eV cell^{-1})	0.000	0.514	1.899	0.077	0.287	0.039

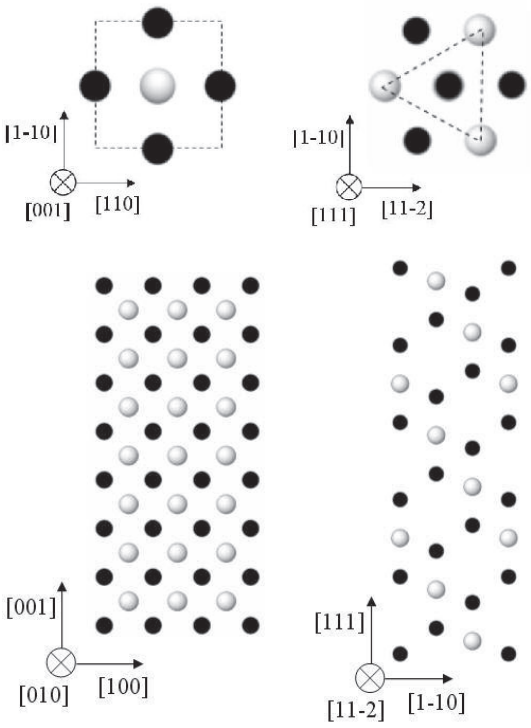

Figure 6. Top and side views of the un-relaxed (100) and (111) surfaces of c-HfO_2. Black dots represent oxygen and gray dots hafnium atoms.

Hf-terminated surfaces become comparable in energy. The difference in the surface energies of the c-$(100)_{\text{O}}$ and c-$(111)_{\text{O}}$ surfaces is very low.

The relaxation patterns for the surfaces of the cubic phase are essentially the same as for tetragonal HfO_2: the top layer relaxes inward, the subsurface layer relaxes slightly outward, the relaxation is more pronounced on the O-terminated surfaces than on the surface exposing the metal atoms. For all surfaces, we have performed both non-magnetic and spin-polarized calculations. While the Hf- and single O-terminated surfaces are clearly non-magnetic, surface-induced ferromagnetic moments are formed on the double O-terminated (OO-terminated) surfaces. On the corrugated c-$(111)_{\text{OO}}$ surface, we calculate magnetic moments of 1.363 and $0.436\mu_{\text{B}}$ for the two inequivalent O-atoms in the surface layer (the larger moment is located on the outer O-atom), while both O-atoms in the unit cell of the flat c-$(100)_{\text{OO}}$ surface have a moment of $0.732\mu_{\text{B}}$. The Hf atoms in the subsurface layers carry small moments of $-0.041\mu_{\text{B}}$ (111) and $-0.075\mu_{\text{B}}$ (100), respectively, oriented antiparallel to the moments of the surface

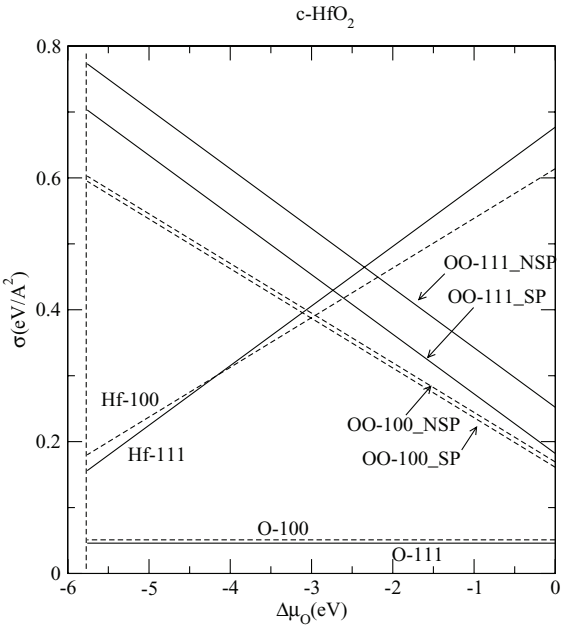

Figure 7. Surface free energies of the polar (100) and (111) surfaces of cubic HfO_2 as a function of the oxygen chemical potential. Results for a Hf-terminated surface and for surfaces covered by a full monolayer of oxygen (OO-termination) and half a monolayer of oxygen (O-termination) are shown. For the OO-terminated surfaces both a non-magnetic and a ferromagnetic surface has been considered. Vertical lines represent the upper and lower limits of the chemical potential (cf text).

O atoms. A weak magnetization of about $0.1\mu_B$ subsist in the second O-layer. The magnetic energy difference is much larger ($\Delta E_{mag} = 1.55\,eV\,cell^{-1}$) for the (111) than for the (100) surface ($\Delta E_{mag} = 0.21\,eV\,cell^{-1}$). In both cases, the gain in magnetic energy is not sufficient to stabilize the ferromagnetic double-oxygen terminated surface with respect to the partially reduced surface.

4.2.2. Magnetic and electronic properties of Hf- and O-terminated surfaces. The analysis of the layer-resolved DOSs (not shown here) demonstrates that the effects leading to surface-ferromagnetism on the fully O-covered surfaces are the same as those discussed for tetragonal HfO_2: the stable O-terminated surface is insulating and non-magnetic due to the complete filling of the O-2p states of the atoms in the surface layer, while for the OO-terminated surface the formation of holes in the valence band induces an exchange-splitting and the formation of a half-metallic and ferromagnetic surface.

5. Influence of point defects on the surface properties of tetragonal HfO_2

The results discussed so far have demonstrated that on fully O covered surfaces of both cubic and tetragonal HfO_2 exchange-splitting of the incompletely filled O-2p band induces surface-ferromagnetism. However, the statistical–mechanical analysis shows that these surfaces are

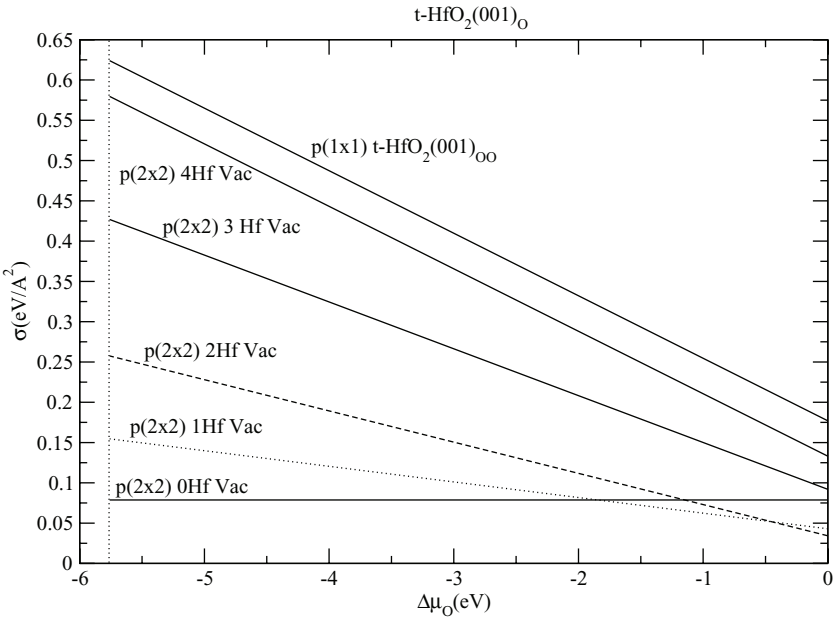

Figure 8. Surface free energies of the single-O terminated (001) surface of tetragonal HfO_2 with vacancies in the subsurface Hf-layer as a function of the oxygen chemical potential. The calculations have been performed for $p(2 \times 2)$ cells containing between 1 and 4 Hf atoms per layer. For surfaces with vacancies or a full oxygen coverage the results are based on spin-polarized calculations, while the single-O-terminated surface is non-magnetic. Vertical lines represent the upper and lower limits of the chemical potential (cf text).

thermodynamically unstable even under highly oxidizing conditions. As the creation of holes in the valence band can also result from the formation of near-surface Hf vacancies, we investigate in the following their influence on the stability and magnetic properties of the (100) surface of tetragonal HfO_2. These calculations have been performed with a (2×2) surface cell containing 4 Hf or 8 oxygen atoms, all other parameters are the same as for the calculations with a (1×1) cell.

5.1. Hf subsurface-vacancies on O-terminated surfaces

In a first set of calculations, we start with a symmetric slab representing the single-O terminated t-$(001)_O$ surface. Hf vacancies are created in the subsurface layer on one side of the slab only. The asymmetry of the slab with Hf-vacancies requires dipole-corrections to eliminate the spurious electrostatic field created by the periodic repetition of the slab. The upper half of the slab containing the vacancies is allowed to relax, whereas the atoms in the lower half remain frozen in their equilibrium positions in the relaxed stoichiometric slab.

Figure 8 shows the variation of the surface energy with the chemical potential of oxygen, calculated for one to four Hf subsurface vacancies. Without vacancies the slab has bulk-like stoichiometry, while if all Hf atoms in the subsurface layer are eliminated, the stoichiometry is the same as in a slab representing the t-$(001)_{OO}$ surface. Quite remarkably, for vacancy concentrations of up to 50%, the formation of Hf vacancies is energetically favored under oxidizing conditions.

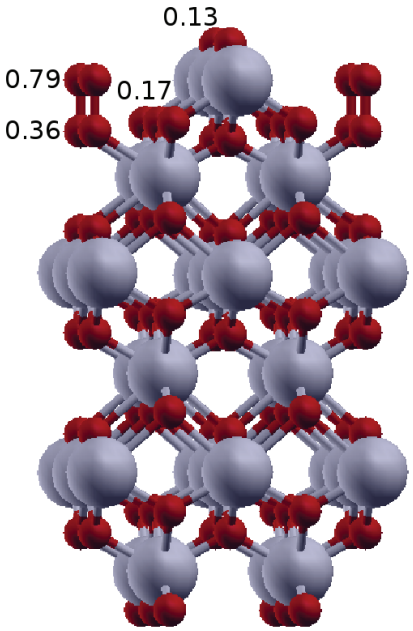

Figure 9. Relaxed atomic geometry of a slab representing the single-O-terminated (001) surface of tetragonal HfO_2 with 50% Hf-vacancies in the upper subsurface Hf-layer (two Hf vacancies per cell). Hf atoms are represented by large gray (light) balls, O atoms by small red (dark) balls. Surface oxygen atoms occupy either bridging sites between Hf atoms or form O_2-groups with O atoms in deeper layers. Numbers attached to O atoms give the local magnetic moment (in μ_B) (cf text).

Figure 9 shows the relaxed atomic geometry for a surface with 50% Hf vacancies in the subsurface layer. Out of the four oxygen atoms per cell in the surface layer, two occupy bridging sites between the remaining subsurface Hf atoms, while the other two oxygen atoms form bonds with oxygen atoms in the fully occupied oxygen layer below the Hf layer, forming O_2 dumbells with an O–O distance of about 1.5 Å. With increasing Hf vacancy concentration, the number of bridging O-atoms is decreased and the concentration of O_2 groups is increased. Figure 8 shows that rather strongly oxidizing conditions stabilize the surface O_2 groups, while at reducing conditions the desorption of O_2 molecules is an exothermic process. It is interesting that even if all Hf atoms are eliminated from the subsurface layer, the resulting surface with a 50/50 coverage of bridging oxygens and O_2 groups is energetically still favored over the fully OO-terminated surface.

The creation of Hf vacancies leads to the formation of holes in the O-2p dominated valence band and to the formation of magnetic moments on the near surface oxygen atoms. The magnetic moment on an O-atom depends on the number of vacant Hf sites in nearest-neighbor positions and on the O–Hf distances. In the defect-free surface, the distance from a Hf atom to an O atom in the uppermost layer is 2.02 Å, to an O atom in the deeper layer the distance is 2.46 Å (cf table 3). On a surface O-atom having lost two Hf neighbors at 2.02 Å we find the largest moment of $0.79\mu_B$, on the lower O atom in the O_2 dumbbell with two vacant Hf sites at 2.46 Å, the magnetic moment is $0.36\mu_B$. A subsurface O atom having lost one Hf neighbor at 2.46 Å has a magnetic moment of $0.17\mu_B$ and even a surface O atom with still two

Table 5. Local magnetic moments on near-surface oxygen atoms on a single-O terminated HfO_2 surface with subsurface Hf-vacancies and total magnetic moment per cell (both in μ_B) and magnetization density per surface area (in μ_B Å^{-2}). Oxygen sites are characterized by the numbers (n, m) of Hf vacancies at distances of 2.02 and 2.46 Å, respectively.

Vacancies	1 Hf	2 Hf	3 Hf	4 Hf
(2,0)		0.79	1.29	1.86
(0,2)	–	0.36	0.13	0.61
(1,0)	0.01	0.17	−0.37	–
(0,1)	0.01	–	0.10	–
–	–	–	0.14	–
(0,0)	0.02	0.13	0.23	0.08
Tot. Moment	0.11	3.45	5.04	14.62
Magnetiz. density	0.002	0.07	0.10	0.28

Hf-neighbors has a magnetic moment of $0.13\mu_B$. The surface magnetization density is $0.07\mu_B$ Å^{-2}. Table 5 summarizes the local magnetic moments, the total magnetic moment per cell and the magnetization density per surface area as a function of vacancy concentration.

Moment formation depends on the local vacancy concentration. With only one Hf vacancy per cell, the surface remains almost non-magnetic (magnetization density $\leqslant 0.002\mu_B$ Å^{-2}), at two Hf vacancies per cell, the magnetization increases to $0.07\mu_B$ Å^{-2}. Stronger magnetic moments are calculated for very high vacancy concentrations (note that the magnetic moments on the O_2 dumbbells approach those of a free O_2 molecule), but these are irrelevant because these surfaces are unstable against desorption of molecular oxygen. The investigation of the electronic structure shows that again magnetic moment formation is driven by the creation of holes in the O-2p band.

5.2. Hf vacancies on Hf-terminated surfaces

We have also briefly investigated the formation of vacancies on the Hf-terminated t-$(001)_{Hf}$ surface. In the oxidizing limit, the formation of one Hf-vacancy per $p(2 \times 2)$ cell lowers the surface energy by 0.15 eV Å^{-2}, of two Hf vacancies by 0.25 eV Å^{-2}, no further reduction occurs for higher vacancy concentrations. But even in these cases, the Hf-terminated surfaces have a higher energy than both oxygen terminated surfaces. Under strongly reducing conditions, the formation of one or two vacancies per cell is a slightly exothermic reaction (with an energy gain of about 0.04 eV Å^{-2}), higher vacancy concentrations are energetically unfavorable. Vacancy formation induces a weak magnetic moment on the remaining Hf surface atoms. At one Hf vacancy per cell, the remaining three Hf atoms carry magnetic moments of 0.20, 0.33 and $0.31\mu_B$, respectively, corresponding to an overall magnetization density of $0.02\mu_B$ Å^{-2}. However, the defective Hf-terminated surfaces remain energetically disfavored relative to oxygen terminated surfaces.

6. Conclusions

We have presented *ab initio* investigations of low-index surfaces of the tetragonal and cubic phases of HfO_2. *Ab initio* statistical mechanics in combination with DFT total energy calculations have been used to determine the stable surface terminations. For both polymorphs we find that on these polar surfaces, a partially reduced surface covered by half a monolayer of oxygen is lower in energy than the Hf- and fully O-terminated surfaces at all realistic values of the chemical potential of oxygen. However, under oxidizing conditions, the formation of subsurface Hf vacancies below the top oxygen layer is found to be favored on the partially reduced t-$(001)_O$ surface. This has important consequences on the electronic and magnetic properties of the surfaces. Hf-terminated surfaces are metallic and non-magnetic, fully O-terminated surfaces are half-metallic and ferromagnetic, the partially reduced single O-terminated surfaces are insulating and non-magnetic. Magnetic moments are formed also on the O-atoms of the single-O-terminated surface with subsurface Hf vacancies. The formation of magnetic moments on the surfaces covered by a completed monolayer of oxygen is driven by the formation of holes in the O-2p valence band and the combined effect of Coulomb repulsion between the holes and Hund's rule coupling. The calculated magnetic moments of the ferromagnetic surfaces are about $0.13\mu_B$ Å^{-2}, which is significantly lower than the values of 1–$4\mu_B$ Å^{-2} reported by Coey [11, 17]. Likewise, the magnetism of the single-O-terminated surface with Hf subsurface vacancies is driven by the formation of holes in the O-2p valence band. But again, on the thermodynamically stable surfaces with a maximum Hf vacancy concentration of 50% in the subsurface layer, the surface magnetization density of $0.07\mu_B$ Å^{-2} is far too low compared with experiment.

However, our analysis leads to interesting parallels between the mechanism leading to the formation of surface-induced magnetic moments and other explanations put forward to explain the ferromagnetism of HfO_2. Pemmaraju and Sanvito [19] have reported that ferromagnetism in HfO_2 is driven by Hf vacancies, while Weng and Dong [22] have proposed that hole-doping (i.e. substitution of Hf by an element with a lower number of valence electrons) can cause the formation of a magnetic moment on the oxygen atoms surrounding the defect. In both cases, the presence of the defect leads to the formation of holes in the O-2p band, which undergoes an exchange splitting. Hence, the mechanisms for moment formation in bulk HfO_2 with defects is the same as on the O-rich surfaces. Unfortunately these studies have not considered the energetics of defect formation—hence, it remains unknown whether the defects driving moment formation are likely to be formed at all. Very recently, Zheng *et al* [56] have performed an extensive first-principles study of native point defects in hafnia and zirconia. Defect formation energies for oxygen and metal vacancies, oxygen and metal interstitials, and of anti-site defects have been calculated as a function of the chemical potentials of both constituents and of the position of the Fermi level. In the present context, the important result is that neutral Hf vacancies (as postulated by Pemmaraju and Sanvito) have a high energy of formation. Thus, DFT calculations predict both magnetic oxygen-terminated surfaces and Hf vacancies to be less stable than the non-magnetic surfaces and defects creating an oxygen deficiency. Our investigations of the formation of subsurface Hf vacancies below the top O-layer of the stable t-$(001)_O$ surface suggest a cooperative effect between surface formation and the formation of Hf vacancies: at least under oxidizing conditions Hf vacancy formation is even energetically favored in the near-surface region. This conjecture is also supported by the recent discovery [57] that in ZnO surfaces doping with Co not only enhances ferromagnetism, but also contributes to

the stability of the surface. Thus the interplay between defect formation and surface could be a mechanism to explain some of the controversial results on dilute magnetic oxides. Of course the present investigation is only a first step—future investigations will have to be performed on larger surface cells and thicker slabs and allow for changes in the local stoichiometry also in deeper layers to eventually account for the experimentally measured magnetization densities. This will require a strongly increased computational effort, but seems to be a promising line of research.

It should also be mentioned that the proposed mechanism for the formation of a 'd^0 ferromagnetism' or 'p-wave ferromagnetism' driven by the Coulomb repulsion between holes in incompletely filled p-bands is not restricted to dielectric oxides. Recently, it has been proposed that zinc-blende or wurtzite-type compounds formed by an alkaline-earth metal (Ca, Sr) and a group V element (P, As, Sb) are ferromagnetic with moments carried by the exchange-split p-bands of the pnictide element [58, 59]. However, the problematic point is again the energetics—it remains to be demonstrated that these compounds are sufficiently stable to allow them to be synthesized.

Acknowledgments

The Madrid–Vienna cooperation has been initiated by a Marie-Curie Fellowship for J I Beltrán in the MC-Training Site 'Atomic-scale computational materials science' at the Universität Wien. Partial support by the Spanish Ministerio de Educación y Ciencia under contract no MAT2006-05122 is gratefully acknowledged.

References

[1] Wilk G, Wallace R M and Anthony J M 2001 *J. Appl. Phys.* **89** 5243
[2] Fonseca L R C, Demkov A A and Knizhnik A 2003 *Phys. Status Solidi* b **239** 48
[3] Robertson J 2006 *Rep. Prog. Phys.* **69** 327
[4] Ginley D S and Bright C 2000 *MRS Bull.* **25** 15
[5] Diebold U 2003 *Surf. Sci. Rep.* **48** 53
[6] Batzill M and Diebold U 2005 *Prog. Surf. Sci.* **79** 47
[7] Matsumoto Y, Murakami M, Shono T, Hasegawa T, Fukumura T and Kawasaki M 2001 *Science* **291** 854
[8] Wang Z, Wang W, Tang J, Tung L D, Spinu L and Zhou W 2003 *Appl. Phys. Lett.* **83** 518
[9] Ogale S B *et al* 2003 *Phys. Rev. Lett.* **91** 77205
[10] Venkatesan M, Fitzgerald C B, Lunney J G and Coey J M D 2004 *Phys. Rev. Lett.* **93** 177206
[11] Coey J M D 2005 *J. Appl. Phys.* **97** 10D313
[12] Coey J M D 2006 *Curr. Opin. Solid State Mater. Sci.* **10** 83
[13] Venkatesan M, Fitzgerald C B and Coey J M D 2004 *Nature* **430** 630
[14] Kittilstved K R, Liu W K and Gamelin D R 2006 *Nat. Mater.* **5** 29
[15] Coey J M D 2005 *Solid State Sci.* **7** 660
[16] Sundaresan A, Bhargavi R, Rangarajan N, Siddesh U and Rao C N R 2006 *Phys. Rev.* B **74** 161306
[17] Coey J M D, Venkatesan M, Stamenov P, Firtgerald C B and Dorneles L S 2005 *Phys. Rev.* B **72** 024450
[18] Hong N H, Sakai J, Poirot N and Brizé V 2006 *Phys. Rev.* B **73** 132404
[19] Pemmaraju C D and Sanvito S 2005 *Phys. Rev. Lett.* **94** 217205
[20] Stoneham A M 1975 *Theory of Defects in Solids* (Oxford: Clarendon) chapter 16
[21] Efimov I S, Yunoki S and Sawatzki G A 2002 *Phys. Rev. Lett.* **89** 216403
[22] Weng H and Dong J 2006 *Phys. Rev.* B **73** 132410

[23] Makarova T L 2004 *Semiconductors* **38** 615
[24] Young D P, Hall D, Torelli M E, Fisk Z, Sarrao J L, Thomson J D, Ott H R, Oseroff S B, Goodrich R G and Zysler R 1999 *Nature* **397** 412
[25] Gallego S, Beltrán J I, Cerdá J and Munoz M C 2005 *J. Phys.: Condens. Matter* **17** L451
[26] Mukhopadhyay A B, Sanz J F and Musgrave C B 2006 *Phys. Rev.* B **73** 115330
[27] Tkachev S N, Manghnani M H, Niilisk A, Aarik J and Mandar H 2005 *J. Mater. Sci.* **40** 4293
[28] Tkachev S N, Manghnani M H, Niilisk A, Aarik J and H Mändar 2005 *Spectrochim. Acta* A **61** 2434
[29] Kresse G and Hafner J 1993 *Phys. Rev.* B **48** 13115
[30] Kresse G and Furthmüller J 1996 *Comput. Mater. Sci.* **6** 15
[31] Kresse G and Furthmüller J 1996 *Phys. Rev.* B **54** 11169
[32] Blöchl P 1994 *Phys. Rev.* B **50** 17 953
[33] Kresse G and Joubert D 1999 *Phys. Rev.* B **59** 1758
[34] Perdew J P, Burke K and Ernzerhof M 1996 *Phys. Rev. Lett.* **77** 3865
[35] Monkhorst H J and Pack J D 1972 *Phys. Rev.* B **13** 5188
[36] Vosko S H, Wilk L and Nusair M 1980 *Can. J. Phys.* **58** 1200
[37] Liu L G 1979 *Earth Planet. Sci. Lett.* **44** 390
[38] Haines J, Leger J M and Atouf A 1995 *J. Am. Ceram. Soc.* **78** 445
[39] Jaffe J E, Bachorz R A and Gutowski M 2005 *Phys. Rev.* B **72** 144107
[40] Kang J, Lee E C and Chang K J 2003 *Phys. Rev.* B **68** 054106
[41] Zhao X and Vanderbilt D 2002 *Phys. Rev.* B **65** 233106
[42] Foster A S, Lopez Gejo F, Shluger A L and Nieminen R M 2002 *Phys. Rev.* B **65** 174117
[43] Adams D M, Leonard S, Russel D R and Cernik R J 1991 *J. Phys. Chem. Solids* **52** 1181
[44] Stacy D W, Johnstone J K and Wilder D R 1972 *J. Am. Ceram. Soc.* **55** 482
[45] Wang J, Li H P and Stevens R 1992 *J. Mater. Sci.* **27** 5397
[46] Balog M, Schieber M, Michiman M and Patai S 1977 *Thin Solid Films* **41** 247
[47] Oshima M, Toyoda S, Okumura T, Okabayashi J and Kumigashira H 2003 *Appl. Phys. Lett.* **83** 2172
[48] Desgreniers S and Lagarec K 1999 *Phys. Rev.* B **59** 8467
[49] Leger J M, Atouf A, Tomaszweski P E and Pereira A S 1993 *Phys. Rev.* B **48** 93
[50] Perdew J P, Chevary A, Vosko S H, Jackson K A, Pedersen M R, Singh D J and Fiolhais C 1992 *Phys. Rev.* B **46** 6671
[51] Louie S G, Froyen S and Cohen M L 1982 *Phys. Rev.* B **26** 1738
[52] Reuter K and Scheffler M 2002 *Phys. Rev.* B **65** 035406
[53] Eichler A and Kresse G *Phys. Rev.* B **69** 045402
[54] Rohrbach A, Hafner J and Kresse G 2004 *Phys. Rev.* B **69** 075413
[55] Rollmann G, Rohrbach A, Entel P and Hafner J 2004 *Phys. Rev.* B **69** 165107
[56] Zheng J X, Ceder G, Maxisch T, Chim W K and Choi W K 2007 *Phys. Rev.* B **75** 104112
[57] Sanchez N, Gallego S and Munož M C to be published
[58] Kusabe K, Geshi M, Tsukamoto H and Suzuki N 2004 *J. Phys.: Condens. Matter* **16** 5639
[59] Sieberer M, Redinger J, Khmelevskyi S and Mohn P 2006 *Phys. Rev.* B **73** 024404